Received 23 May 2006
Revised 14 January 2008
Accepted 9 April 2008

Prediction of turbulent flow and heat transfer in channels with array of detached and alternative attached-detached ribs

Mehrdad Raisee and Arman Rokhzadi
Department of Mechanical Engineering, Faculty of Engineering, University of Tehran, Tehran, Iran

Abstract

Purpose – The purpose of this paper is to investigate turbulent fluid flow and heat transfer through passages with an array of either detached or alternative attached-detached ribs of square cross-section.

Design/methodology/approach – The finite-volume method in a partially staggered grid system has been applied. For the modeling of turbulence, the zonal as well as the linear and non-linear low-Reynolds number k–ε models have been employed.

Findings – The numerical results show that the presence of the ribs produces a very complex flow in the channel. The mean flow predictions for the channel with detached ribs show that the low-Re k–ε models are able to reproduce most of the experimentally observed flow features away from the ribbed wall, but return lower stream-wise velocities close to the wall. Additionally, all low-Re k–ε models underpredict the stream-wise turbulence intensity whilst producing correct cross-stream turbulence intensity levels close to the measured data. All three turbulence models fail to completely reproduce the distribution of Nusselt number. Among three turbulence models examined in this work, the zonal k–ε model produces the best heat transfer predictions.

Originality/value – The work contributes in understanding of the flow and thermal development in passages with detached ribs. The present set of 2D and steady heat and fluid flow comparisons establishes a base-level for more realistic three-dimensional and unsteady computations. The results of this study may be of interest to engineers attempting to re-design the internal cooling system of gas turbine blades and to researchers interested in the turbulent flow-modification aspects of heat transfer enhancement of forced convection in ribbed passages.

Keywords Flow, Heat transfer, Turbulence, Modelling
Paper type Research paper

Nomenclature

A	= Cross-section area
H	= Rib height
B	= Half of channel height
K	= Turbulent kinetic energy
Nu	= Nusselt number
Nu_{fd}	= Nusselt number in fully developed smooth channel flow
Pr	= Molecular Prandtl number
q''_w	= Local surface heat flux on the wall
Re	= Reynolds number
U_i	= Mean velocity components (U,V)
$\overline{u_i\theta}$	= Turbulent heat fluxes
W	= Rib width
x_i	= Cartesian coordinate (x,y)
Yap	= Original algebraic form of the Yap term as proposed by Yab

The authors would like to thank the University of Tehran for providing financial support for this study.

International Journal of Numerical Methods for Heat & Fluid Flow
Vol. 19 Nos. 3/4, 2009
pp. 266-284

0961-5539
DOI 10.1108/09615530910938281

Greek letters

Θ_b = Cross-section averaged fluid temperature

Θ_w = Wall temperature

$\tilde{\varepsilon}$ = Isotropic dissipation rate

δ_{ij} = Kronecker delta

Θ = Temperature

1. Introduction

Heat transfer enhancing ribs are widely used in many industrial applications such as the cooling passages of gas turbine blades, gas-cooled nuclear reactor and heat exchangers. Though such rib-tabulators substantially enhance the overall heat transfer, the heat transfer coefficient is locally reduced immediately in the corner region downstream of each rib forming hot spots. To eliminate such hot spots, one can replace the attached ribs with the detached ones. In this paper, this idea is numerically studied by computing flow and heat transfer through channels with arrays of either detached or alternative attached-detached ribs (see Figure 1). Flow and heat transfer through passages with attached ribs have been topic of numerous experimental and numerical investigations. Examples of experimental work are Webb *et al.* (1971), Han (1988) and Liou and Hwang (1992). Most of the reported computational efforts (Lee *et al.*, 1988; Liou *et al.*, 1993) employed high-Reynolds-number k–ε turbulence model with wall-functions for their predictions. However, it is known that such models are unsuitable for cases that there is flow separation. Iacovides and Raisee (1999) considered flow and heat transfer through two and three-dimensional rib-roughened passages with normal ribs in "in-line" and "staggered" arrangements using the zonal and low-Re k–ε and DSM models. The results of these studies showed that the most reliable flow and thermal predictions are produced through the use of low-Reynolds number second-moment closures. In a subsequent study, Iacovides and Raisee (2000) have employed low-Reynolds-number k–ε models to investigate flow and heat transfer in two-dimensional and axi-symmetric rib roughened passages. The results of their study showed that fairly accurate heat transfer predictions can be produced by adding a differential length-scale correction source term to the dissipation rate equation of the low-Re k–ε model. Tsia *et al.* (2000) employed low-Reynolds-number k$-\varepsilon$, k–ω and k–ε–v^2 models for numerical computation of 2D fluid flow and heat transfer in a channel with stream-wise periodic ribs mounted on one of the principal walls. They found that the k–ω model leads to too low heat transfer and turbulence intensity levels. Among k–ε models, Lin and Hwang (1998) turbulence model with the Yap length scale correction term (Yap, 1987) produced the best heat transfer levels. Durbin's (1995) k–ε–v^2 model with the Yap term exhibited further improvement. More recently, Raisee *et al.* (2004) applied the modified low-Re non-linear k–ε model of Craft *et al.* (1999) to the prediction of flow and heat transfer in two-dimensional and axi-symmetric rib-roughened passages and found that marked improvements in thermal predictions can be achieved in comparison to the original version of non-linear k–ε proposed by Craft *et al.* (1993). Moreover, the replacement of the "Yap" correction term with the "NYP" (differential length-scale correction term proposed by Iacovides and Raisee (1999)), further improves the heat transfer predictions of the non-linear k–ε model. Hsieh and Lien (2004) assessed the performance of various low-Re k–ε models on turbulent forced convection in a channel with periodic ribs. The influence of the Yap correction and the non-linear stress-strain relation on the predictions of mean-flow, turbulence quantities and local heat transfer rate is examined. Moreover, the effect of thermal boundary conditions on the heat transfer predictions is investigated by

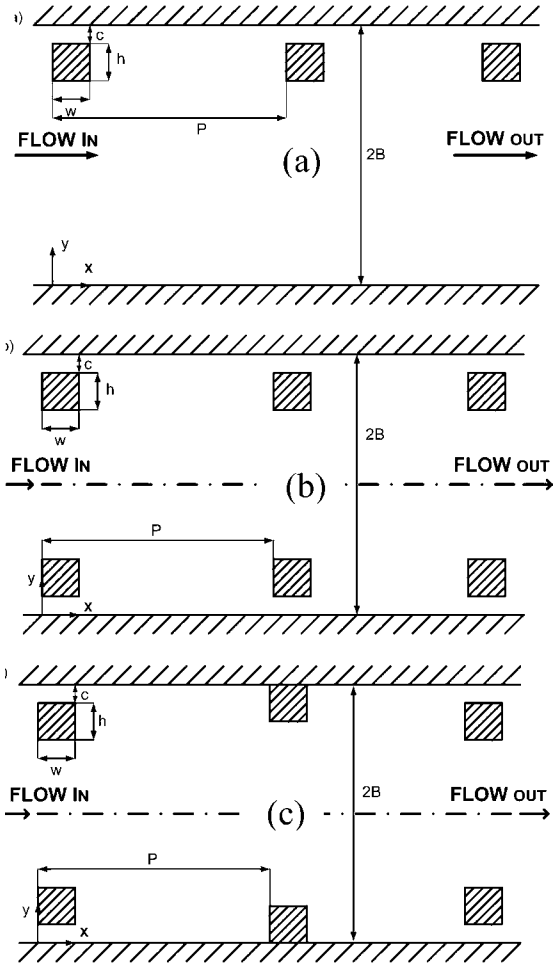

Figure 1.
Schematic of passages examined

employing both the prescribed heat flux approach and the conjugate heat transfer approach. It was found that the inclusion of the Yap correction in the ε-equation significantly improves the predictions of mean velocity and wall heat transfer. The employment of the non-linear stress-strain relation only marginally improves the predictions of turbulence quantities. Wu and Perng (2004) investigated heat transfer enhancement due to flow modification induced by vortex shedding of a rectangular plate turbulator in vertical channel. The large eddy simulation (LES) and SIMPLE-C method coupled with preconditioned conjugate gradient methods have been applied for simulations. Their results showed that the installation of turbulators in cross-flow above an upstream block can effectively enhance the heat transfer performance in a particular width-to-height ratio of turbulator and Grasehof numbers.

The trend in recent years has been to align ribs at an angle to the main flow direction. The resulting vortices move the fluid from the walls to the centre, reducing

the thickness of the boundary layers. Investigations of heat transfer through passages with inclined ribs have already appeared in the scientific literature. Nonino and Comini (2002) have reported numerical result for unsteady 3D laminar flow and heat transfer in ribbed channels with transverse and angled ribs placed on one or two of the walls. They focused on pressure drop and heat transfer characteristic in rib-roughened, square channels for different Reynolds number. They found that in all cases considered, the f Re parameter of the ribbed channels is much higher than the one corresponding to the smooth channel. On the contrary, a significant improvement of the average Nusselt number was observed only for angled ribs, at relatively high values of Reynolds number. Recently, Iacovides and Raisee (2008), using two 2-layer models of turbulence (an effective-viscosity model and a second-moment closure), have reported numerical results for water flow through a straight, orthogonally rotating duct, with ribs along the leading and trailing walls, in a staggered arrangement and at an angle of 45° to the main flow direction. The flow and thermal developments were found to be dominated by the rib-induced secondary motion. The thermal predictions, especially those of the second-moment closure, reproduced the levels and most of the local features of the measured Nusselt number.

Compare to the volume of the reported studies for passages with attached ribs, only a limited number of studies investigated turbulent flow and heat transfer in passages with detached ribs. Liou and Wang (1995) measured turbulent heat transfer characteristics in a rectangular duct with an array of square ribs detached from the duct wall with a fixed rib clearance of c/h = 0.58 by using holographic interferometery. They found that by lifting the ribs from the wall, the local heat transfer deterioration behind the rib can be effectively removed. Liou *et al.* (1997) reported LDV measurements for mean velocity, turbulence intensity and shear-stress in a duct with detached ribs and were able to identify the main flow features responsible for the occurrence of peak values of heat transfer coefficient around the rib. Tsia and Hwang (1999) conducted an experimental study to measure heat transfer and friction in a rectangular duct with arrays of attached, detached and alternative attached-detached ribs. One main finding in this work was that the entrance length for composite ribs (alternative attached-detached ribs) is longer than that for the fully-attached or fully-detached ribs.

The main objective of this paper is to examine the suitability of the zonal and linear and non-linear low-Re k–ε models in prediction of flow and thermal fields in passages with detached ribs. These models have been previously employed for prediction of convective heat transfer through various two and three-dimensional and axi-symmetric passages with attached ribs by Iacovides and Raisee (2000) and Raisee *et al.* (2004). The results of these studies indicated that the zonal k–ε model underpredicts the wall heat transfer while the linear and non-linear produce more reliable heat transfer levels. The present contribution further examines the effectiveness of these turbulence models in prediction of convective heat transfer in channels with detached ribs.

2. Case examined

In this study, turbulent fluid flow and heat transfer through three types of passages have examined. These passages, as shown in Figure 1, are: (a) a channel with an array of ribs detached from one wall, (b) a channel with arrays of detached ribs close to both walls, and (c) a channel with an array of attached-detached ribs near both walls. As

shown in Figure 1, h denotes the rib-height, w the rib-width, P the rib-pitch, c is rib-clearance and 2B the channel height.

In all test cases, the working fluid is air (Pr = 0.71), the cross-section of the rib is square and the Reynolds number is based on the bulk velocity and hydraulic diameter of channel. The details of these test cases are given in Table I. Flow measurements for the channel with ribs detached from one wall (passage (a)) have been obtained by Liou *et al.* (1997). Heat transfer measurements for the channel with detached or alternative attached-detached ribs close to both walls (passages (b) and (c)) were reported by Tsia and Hwang (1999). For wall thermal boundary conditions a constant heat flux was assumed for the walls of each channel.

For all three cases, the channel aspect-ratio, W/2B, is 4. In this study, the effects of side walls were ignored and computations were performed only in a vertical plane located at the lateral mid-point of the channel. Recent computations of turbulent flow through rectangular ducts of similar aspect ratio by Raisee *et al.* (2006), for which the secondary velocity vectors and stream-wise velocity contours at a section in the developing region are shown in Figure 2, indicates that the side wall effects are insignificant and flow field can be treated as two-dimensional.

The local Nusselt number is defined as:

$$\mathrm{Nu} = \frac{q''_w D_h}{\kappa(\Theta_w - \Theta_b)} \tag{1}$$

where κ is thermal conductivity of the fluid, D_h is the hydraulic diameter, q''_w the wall-heat-flux, Θ_w the wall temperature and Θ_b the cross-section averaged fluid temperature which is obtained from:

$$\Theta_b = \frac{\int_A \Theta U dA}{\int_A U dA} \tag{2}$$

Passage	P/h	h/2B	c/h	Re	Experience data	Comparisons
(a)	10.	0.133	0.38	20,000	Liou *et al.* (1997)	Velocity and turbulence intensity profiles
(b)	10.	0.2	0.5	40,000	Tsia and Hwang (1999)	Local Nusselt number
(c)	10.	0.2	0.5	40,000	Tsia and Hwang (1999)	Local Nusselt number

Table I.
Details of cases examined

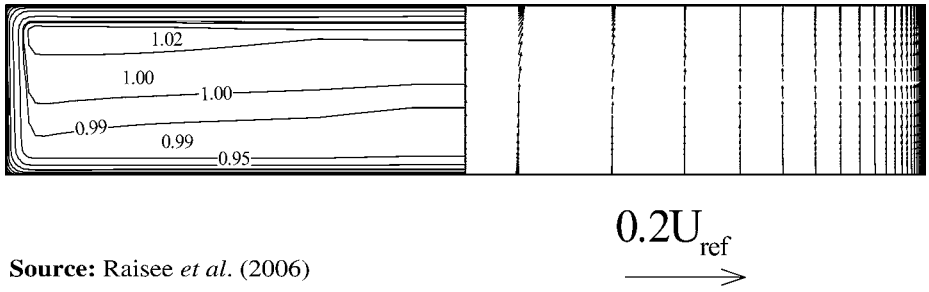

Source: Raisee *et al.* (2006)

Figure 2.
Predicted stream-wise velocity, U/U_{in}, contours (left) and secondary flow vectors (right) for developing turbulent flow through a rectangular cross-section channel, using the non-linear k–ε model

3. Governing equation

All the flow equations are presented in Cartesian notation.

3.1 Mean flow equations

For a steady incompressible flow, the conservation laws of mass, momentum and energy may be written as:

$$\text{Continuity:} \qquad \frac{\partial U_j}{\partial x_j} = 0 \tag{3}$$

$$\text{Momentum:} \qquad \frac{\partial (U_i U_j)}{\partial x_j} = -\frac{1}{\rho}\frac{\partial P}{\partial x_i} + \frac{\partial}{\partial x_j}\left(\nu \frac{\partial U_i}{\partial x_j} - \overline{u_i u_j}\right) \tag{4}$$

$$\text{Energy:} \qquad \frac{\partial (U_j \Theta)}{\partial x_j} = \frac{\partial}{\partial x_j}\left(\frac{\nu}{Pr}\frac{\partial \Theta}{\partial x_j} - \overline{u_j \Theta}\right) \tag{5}$$

where Pr is Prandtl number of fluid.

4. Turbulence modelling equation

The turbulence models employed for computation are the zonal k–ε/one-equation model, the Launder and Sharma (1974) low-Re k–ε model, and a recently developed version of non-linear low-Re k–ε model (Craft *et al.*, 1999). In the zonal and linear low-Re k–ε models, the Reynolds stresses and the turbulent heat fluxes are obtained via the well-known effective viscosity and effective diffusivity approximations, respectively, shown in Equations (6) and (7):

$$\overline{u_i u_j} = -\nu_t\left(\frac{\partial U_i}{\partial x_j} + \frac{\partial U_j}{\partial x_i}\right) + 2/3\delta_{ij}k \tag{6}$$

$$\overline{u_i \theta} = -\frac{\nu_t}{\sigma_\theta}\frac{\partial \Theta}{\partial x_i} \tag{7}$$

where σ_θ is turbulent Prandtl number and its value is given in Table II.

4.1 Zonal k–ε *one-equation model*

In this turbulence model, the computational domain is divided into two parts: namely fully turbulent region and low-Re near wall region. In the fully turbulent region the standard high-Re version of the k–ε model is used, while in the near-wall region a low-Re version of a one-equation model of k-transport is employed. This approach allows the resolution of the mean flow across the viscous wall sub-layer, without the need to use a very fine near-wall grid. In the fully turbulent region the turbulent viscosity (ν_t)

c_μ	$c_{\varepsilon\,1}$	$c_{\varepsilon\,2}$	σ_k	σ_ε	σ_θ
0.09	1.44	1.92	1.0	1.22	0.9

Table II.
Empirical constants for the k–ε model

that appears in Equations (6) and (7) is obtained from the turbulent kinetic energy, k, and its dissipation rate, ε , according to Equation (8):

$$\nu_t = c_\mu \frac{k^2}{\varepsilon} \tag{8}$$

Two additional transport equations are solved to evaluate the distributions of k and ε, Equations (9) and (10), respectively:

$$\frac{\partial}{\partial x_j}(U_j k) = \frac{\partial}{\partial x_j}\left[\left(\nu + \frac{\nu_t}{\sigma_k}\right)\frac{\partial k}{\partial x_j}\right] + P_k - \varepsilon \tag{9}$$

$$\frac{\partial}{\partial x_j}(U_j \varepsilon) = \frac{\partial}{\partial x_j}\left[\left(\nu + \frac{\nu_t}{\sigma_\varepsilon}\right)\frac{\partial \varepsilon}{\partial x_j}\right] + c_{\varepsilon 1}\frac{\varepsilon}{k}P_k - c_{\varepsilon 2}\frac{\varepsilon^2}{k} \tag{10}$$

In the near-wall region, Equation (9) is still used to obtain the distribution of k, but the dissipation rate, ε, and the turbulent viscosity, ν_t, are obtained from algebraic expressions (11) and (12), proposed by Woolfshtein (1969), that rely on prescribed length scales $\ell_\varepsilon, \ell_\mu$:

$$\varepsilon = k^{3/2}/\ell_\varepsilon \tag{11}$$

and

$$\nu_t = c_\mu \ell_\mu \sqrt{k} \tag{12}$$

The length scales $\ell_\varepsilon, \ell_\mu$ are obtained from the near-wall distance y, according to:

$$\ell_\varepsilon = 2.55y[1 - \exp(-0.236y^*)] \tag{13}$$

$$\ell_\mu = 2.55y[1 - \exp(-0.016y^*)] \tag{14}$$

where $y^* \equiv yk^{1/2}/\nu$ is the dimensionless wall distance and is used to introduce the damping effect of the wall on turbulence.

4.2 Linear low-Re k–ε *model*

This is an extension of the high-Re k–ε that reproduces the wall damping of turbulence and hence can be used across the viscous sub-layer. The expression for the turbulent viscosity, Equation (15), now includes the damping function f_μ, given by Equation (16), in which the damping parameter, R_t, is the local Reynolds number of turbulence, defined as $\tilde{R}_t = k^2/\nu\tilde{\varepsilon}$:

$$\nu_t = c_\mu f_\mu \frac{k^2}{\tilde{\varepsilon}} \tag{15}$$

$$f_\mu = \exp\left[-3.4/\left(1 + 0.02\tilde{R}_t\right)^2\right] \tag{16}$$

where the variable $\tilde{\varepsilon}$ is the homogeneous dissipation rate which can be related to the real dissipation rate through:

$$\tilde{\varepsilon} = \varepsilon - 2\nu\left(\frac{\partial\sqrt{\mathrm{k}}}{\partial \mathrm{x_j}}\right)^2 \tag{17}$$

The last term in the k-transport Equation, (18), the only difference between the high-Re and low-Re versions of this equation, ensures that at the wall the dissipation of turbulence remains finite. One difference between the high-Re and low-Re versions of the ε equation, Equations (10) and (19), respectively, is the E term which represents the direct effects of viscosity on the larger, energy-containing turbulent eddies and was first introduced by Jones and Launder (1972) and is expressed as Equation (20):

$$\frac{\partial}{\partial \mathrm{x_j}}\left(\mathrm{U_j k}\right) = \frac{\partial}{\partial \mathrm{x_j}}\left[\left(\nu + \frac{\nu_\mathrm{t}}{\sigma_\mathrm{k}}\right)\frac{\partial k}{\partial \mathrm{x_j}}\right] + \mathrm{P_k} - \tilde{\varepsilon} - 2\nu\left(\frac{\partial\sqrt{\mathrm{k}}}{\partial \mathrm{x_j}}\right)^2 \tag{18}$$

$$\frac{\partial}{\partial \mathrm{x_j}}\left(\mathrm{U_j}\tilde{\varepsilon}\right) = \frac{\partial}{\partial \mathrm{x_j}}\left[\left(\nu + \frac{\nu_\mathrm{t}}{\sigma_\varepsilon}\right)\frac{\partial \tilde{\varepsilon}}{\partial \mathrm{x_j}}\right] + \mathrm{f_1 c_{\varepsilon 1}}\frac{\tilde{\varepsilon}}{\mathrm{k}}\mathrm{P_k} - \mathrm{f_2 c_{\varepsilon 2}}\frac{\tilde{\varepsilon}^2}{\mathrm{k}} + \mathrm{E} + \mathrm{S}_\varepsilon \tag{19}$$

$$\mathrm{E} = 2\nu\nu_\mathrm{t}\left(\frac{\partial^2 \mathrm{U_i}}{\partial \mathrm{x_j}\partial \mathrm{x_k}}\right)^2 \tag{20}$$

The extra source term S_ε, in Equation (19) is known as the Yap (Yap, 1987) correction term. This term addresses the overestimation of near-wall turbulence energy in separated flows. The damping functions $\mathrm{f_1}$ and $\mathrm{f_2}$ for the generation rate of ε are determined with respect to decaying, grid-generated turbulence:

$$\mathrm{f_1} = 1, \mathrm{f_2} = 1 - 0.3\exp\left(-\tilde{\mathrm{R}}_\mathrm{t}^2\right) \tag{21}$$

The model constants are given in Table II.

It is well-known that, in separated flows, the Launder and Sharma version of ε -equation returns excessively high levels of near-wall turbulence. To address this problem, Yap (1987) introduced an extra source term into the dissipation rate equation, "Yap", based on the wall distance, y.

$$\mathrm{S}_\varepsilon = \mathrm{Yap} = 0.83\frac{\tilde{\varepsilon}^2}{\mathrm{k}}\max\left[\left(\ell/\ell_\mathrm{e} - 1\right)\left(\ell/\ell_\mathrm{e}\right)^2, 0\right] \tag{22}$$

where ℓ is the turbulent length-scale $\mathrm{k}^{3/2}/\tilde{\varepsilon}$, the equilibrium length-scale $\ell_\mathrm{e} = 2.55\mathrm{y}$, and y is the distance to the wall.

4.3 Non-linear low-Re k–ε *model*

The above linear eddy-viscosity model exhibits numerous weaknesses, including an inability to capture normal stress anisotropy and insensitivity to stream-line curvature. Second-moment closure models, on the other hand, account for several of the key

features of turbulence that are misrepresented by the linear eddy-viscosity models. However, these models are considerably more complex and require higher CPU time than eddy-viscosity model. A simpler alternative for approximating of the Reynolds stresses is to extend the strain-stress relation of the linear eddy-viscosity model, by adding all the higher order (second and third order) non-linear combinations of the strain and vorticity rate tensors that satisfy the kinematic constraints of the turbulent stress tensor. These non-linear strain-stress relations have the ability to produce the differences between the normal stresses and thus can extend the model's applicability, by allowing it to predict flows in which the anisotropy of turbulence is important, such as flows involving turbulence-driven secondary motions. Suga (1995) developed a non-linear eddy viscosity model (NLEVM) with terms up to cubic order, in order exhibit correct sensitivity to streamline curvature. In this turbulence model, the turbulent stresses are obtained via the constitutive relation, Equation (23):

$$\begin{aligned} a_{ij} = \frac{\overline{u_i u_j}}{k} - \frac{2}{3}\delta_{ij} = & -\frac{\nu_t}{k}S_{ij} + c_1\frac{\nu_t}{\tilde{\varepsilon}}\left(S_{ik}S_{kj} - \frac{1}{3}S_{kl}S_{kl}\delta_{ij}\right) \\ & + c_2\frac{\nu_t}{\tilde{\varepsilon}}\left(\Omega_{ik}S_{kj} + \Omega_{jk}S_{ki}\right) + c_3\frac{\nu_t}{\tilde{\varepsilon}}\left(\Omega_{ik}\Omega_{jk} - \frac{1}{3}\Omega_{lk}\Omega_{lk}\delta_{ij}\right) \\ & + c_4\frac{\nu_t k}{\tilde{\varepsilon}^2}\left(S_{ki}\Omega_{lj} + S_{kj}\Omega_{li}\right)S_{kl} + c_5\frac{\nu_t k}{\tilde{\varepsilon}^2}\left(\Omega_{il}\Omega_{lm}S_{mj}\right. \\ & \left. + S_{il}\Omega_{lm}\Omega_{mj} - \frac{2}{3}S_{lm}\Omega_{mn}\Omega_{nl}\delta_{ij}\right) + c_6\frac{\nu_t k}{\tilde{\varepsilon}^2}S_{ij}S_{kl}S_{kl} + c_7\frac{\nu_t k}{\tilde{\varepsilon}^2}S_{ij}\Omega_{kl}\Omega_{kl} \end{aligned} \tag{23}$$

where S_{ij} and Ω_{ij} are strain and vorticity rate tensors that obtain from Equations (24), respectively:

$$S_{ij} = \left(\frac{\partial U_i}{\partial x_j} + \frac{\partial U_j}{\partial x_i}\right), \quad \Omega_{ij} = \left(\frac{\partial U_i}{\partial x_j} - \frac{\partial U_j}{\partial x_i}\right) \tag{24}$$

The model coefficients, c_1 to c_7, have been calibrated by Craft *et al.* (1993), by reference to several flows, including homogeneous shear flows, swirling flows and curved channel flows. The values of these coefficients are given in Table III The k and $\tilde{\varepsilon}$ transport equations and eddy-viscosity formulation are similar to those of linear model, however, for modelling of c_μ the following expression was proposed by Craft *et al.* (1999).

$$c_\mu = \min\left[0.09, \frac{12}{1 + 3.5\eta + f_{RS}}\right] \tag{25}$$

Table III.
Values of coefficients in the non-linear k–ε model

c_1	c_2	c_3	c_4	c_5	c_6	c_7
−0.1	0.1	0.26	$10c_\mu^2$	0	$-5c_\mu^2$	$5c_\mu^2$

With

$$\eta = \max(\tilde{S}, \tilde{\Omega}) \tag{26}$$

where strain and vorticity invariants are expressed as:

$$\tilde{S} = \frac{k}{\tilde{\varepsilon}}\sqrt{0.5 S_{ij} S_{ij}}, \tilde{\Omega} = \frac{k}{\tilde{\varepsilon}}\sqrt{0.5 \Omega_{ij} \Omega_{ij}} \tag{27}$$

and

$$f_{RS} = 0.235[\max(0, \eta - 3.333)]^2 \exp\left(-\tilde{R}_t/400\right) \tag{28}$$

The viscous damping of ν_t is provided by the function f_μ:

$$f_\mu = 1 - \exp\left\{-\left(\frac{\tilde{R}_t}{90}\right)^{1/2} - \left(\frac{\tilde{R}_t}{400}\right)^2\right\} \tag{29}$$

The near-wall source term E is now expressed as:

$$E = \begin{cases} 0.0022\frac{\tilde{S}\nu_t k^2}{\tilde{\varepsilon}}\left(\frac{\partial^2 U_i}{\partial X_k \partial X_i}\right)^2 & \text{for} \quad \tilde{R}_t \leq 250 \\ 0 & \text{for} \quad \tilde{R}_t > 250 \end{cases} \tag{30}$$

In this model, the length scale correction term (S_ε) is still required in the dissipation rate equation to correct for over-predicted length scales in boundary layers subjected to adverse pressure gradients and in separated flows.

5. Numerical methods

The general form of the governing equations of mean flow, temperature and turbulence fields may be written as:

$$\frac{\partial}{\partial x}(\rho U \varphi) + \frac{\partial}{\partial y}(\rho V \varphi) = \frac{\partial}{\partial x}\left(\Gamma^\varphi \frac{\partial \varphi}{\partial x}\right) + \frac{\partial}{\partial y}\left(\Gamma^\varphi \frac{\partial \varphi}{\partial y}\right) + S^\varphi \tag{31}$$

where φ represents velocity components, temperature and turbulent quantities (k and ε) and x and y are the coordinates in the stream-wise and cross-stream directions respectively. Γ^φ is an effective diffusion coefficient and S^φ denotes the source term in each transport equation.

In the present study the above transport equation is solved using finite-volume methodology in a semi-staggered grid system. In this grid arrangement, both velocity components (U and V) are located at the same nodal position which is staggered in relative to the pressure nodes. All the Reynolds stresses and scalars are stored at the pressures nodes. The Hybrid differencing scheme is used for approximation of the convective terms. The pressure field is linked to the velocity using the well-known SIMPLE pressure correction algorithm. To avoid instability problems associated with pressure-velocity decoupling, the Rhie and Chow (1983) interpolating scheme is also

employed. The cases examined involved channels that are long enough for repeating flow conditions to prevail over each rib interval. Consequently, the numerical flow domain covers only one rib interval, and repeating flow and thermal boundary conditions are applied. The repeating flow boundary conditions are imposed by first applying uniform bulk corrections on velocity and pressure at the exit plane, in order to satisfy the mass continuity, and then setting the entry conditions the same as those at the exit plane. For the thermal field, the temperature distribution at the entry plane is set equal to that at the exit plane, but with a bulk adjustment which maintains a constant temperature at a reference point, within the entry plane. The grid employed for the predictions of case (a) consists of 281 $\times$ 314 nodes in the stream wise (x) and cross stream (y) directions respectively. From 281 grid nodes in x-direction, 65 nodes cover the top wall of the rib and 216 grids are located in the cavity space between successive ribs. In the cross-stream direction, 56 grids cover the height of the rib. 89 grid points are between the wall and the top surface of the rib and 165 cells are positioned between the bottom side of the rib and the smooth wall. The y^+ value for the nodes adjacent to the walls was less than one, ensuring that the near-wall grids are positioned within the viscous sub-layer. For the zonal model computations 20 grid nodes were placed near each solid wall to resolve the low-Reynolds number region. The value of turbulence Reynolds number at the interface between the low-Reynolds number and fully-turbulent regions was around 100. For the case (a) (channel with detached ribs on one wall), the influence of grid refinement on velocity and heat transfer predictions of the linear k–ε model is shown in Figures 3 and 4, respectively. It is seen that the differences between the predicted streamwise velocity profiles and local Nusselt number on the fine (281 $\times$ 314) and medium (141 $\times$ 158) meshes are fairly small indicating that the numerical results are reasonably grid-independent. Thus, results obtained on the (281 $\times$ 314) mesh can be regarded as grid-independent. By considering the grid dependency of case (a) and noting the fact that the spacing ratio of cases (a) and (b) are the same (i.e. P/h = 10.), a computational grid with 141 $\times$ 318 cells is considered for cases (b). In x-direction 39 nodes are on the top side of the rib and the rest are between the repeating ribs. In the y-direction 40 points covers the height of each rib, 79 nodes are in the gap between each rib and the wall. A 219 $\times$ 398 mesh with

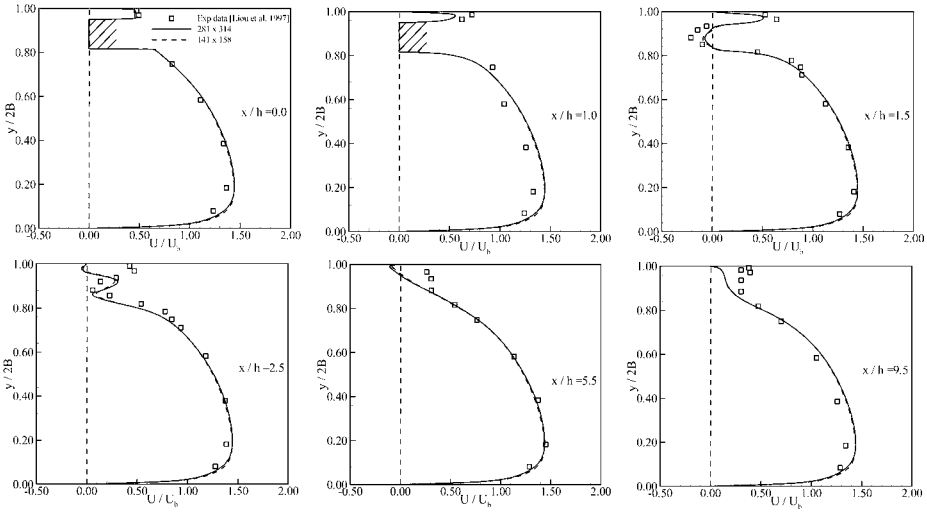

Figure 3.
Stream-wise velocity component profiles for air flow through the channel with detached ribs on one wall (case a)

similar distribution as cases (a) and (b) is used for prediction of third test case. Grid dependency studies performed for cases (b) and (c) also showed that the numerical results presented in this paper are grid-independent.

6. Results and discussion

In Figure 5, the velocity vectors returned by the non-linear k–ε model are compared with those measured by Liou *et al.* (1997). An enlargement of the rib region is also included; to highlight the more interesting features of the flow around the rib. The velocity vectors returned by the zonal and linear k–ε models were similar and thus are not shown here. It is seen that the predicted velocity vectors are qualitatively similar to those measured. The velocity vectors indicate that the shear layers separates

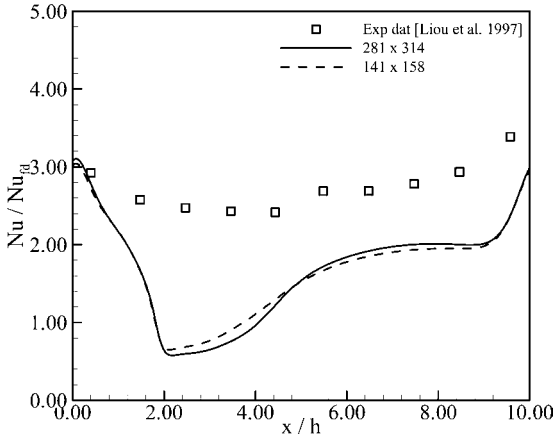

Figure 4.
Distribution of Nusselt number ratio (Nu/Nu_{fd}) for air flow through the channel with detached ribs on one wall (case a)

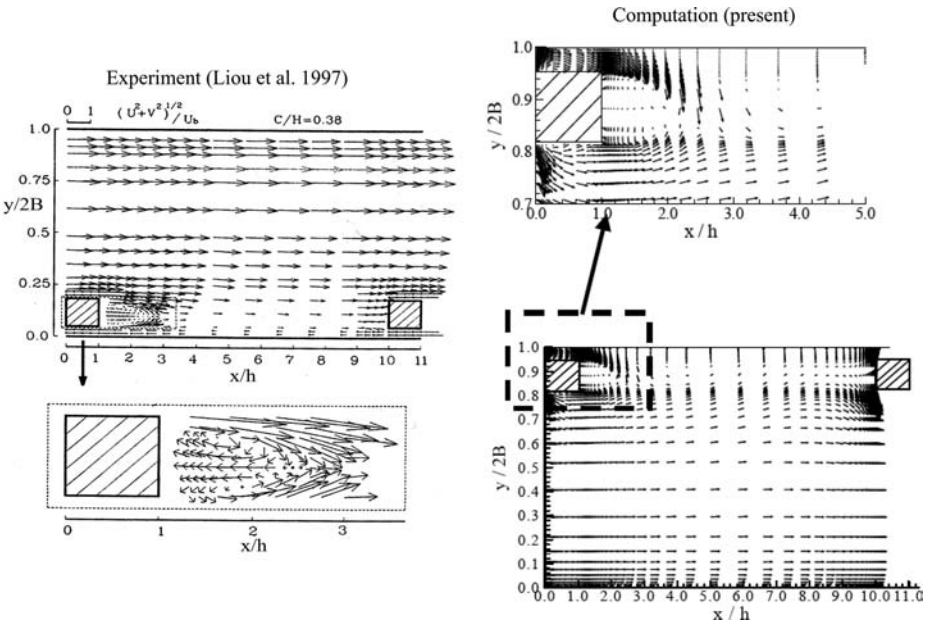

Figure 5.
Mean flow for the channel with detached ribs on one wall (case a)

along both the rib upper and lower surfaces at rib's rear edge to form a wake of about 1.3 rib-heights which is close to 1.35h measured by Liou *et al.* (1997). The non-linear model produces a week recirculating region immediately downstream of the gap region but this behavior in not observed in the experiment.

Comparisons between the predicted and measured stream-wise velocity profiles in Figure 6 show that all turbulence models return similar profiles. While all turbulence models returned acceptable velocity predictions in the core region, they failed correct velocities in the vicinity of the ribbed wall. As can be seen at stations x/h = 2.5, 5.5 and 9.9 the stream-wise velocities are seriously underpredicted.

In Figures 7 and 8 stream-wise and cross-stream turbulence intensities returned by the turbulence models are compared with the measurements of Liou *et al.* (1997). In the core region, while all turbulence models (including the non-linear k–ε model) underpredict the stream-wise turbulence intensity(u'/U_b), the cross-stream intensity

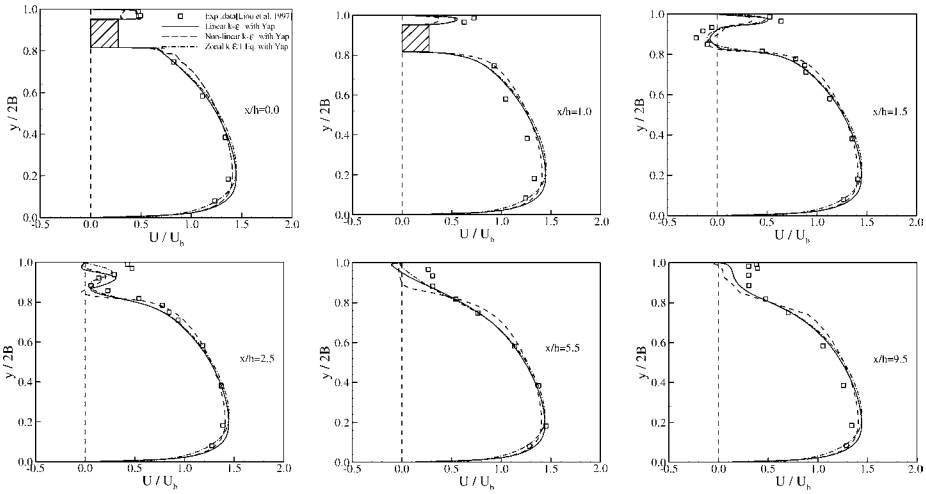

Figure 6.
Stream-wise velocity component profiles for air flow through the channel with detached ribs on one wall (case a)

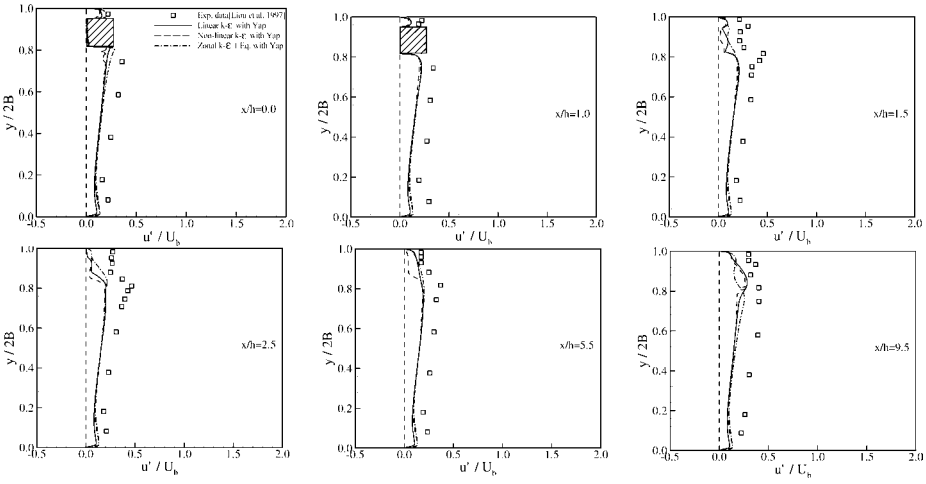

Figure 7.
Stream-wise turbulent intensity profiles for air flow through the channel with detached ribs on one wall (case a)

(v'/U_b) is more faithfully predicted by the turbulence models. Again near the ribbed wall, all k–ε turbulence models (specially the non-linear k–ε model) seriously under predicted the turbulence intensities.

The heat transfer predictions for the first case (passage (a)) using three turbulence models are presented in Figure 9. As can be noted all turbulence models underpredicted local Nusselt number levels. Among the turbulence models, the zonal k–ε model produces the best heat transfer predictions whilst the non-linear k–ε model returns the worst.

In order to investigate reasons behind the differences in distribution of local Nusselt number of turbulence models, the profiles of normalized turbulent kinetic energy and temperature in the vicinity of the ribbed wall are shown in Figures 10-12. As can be noted, among the three turbulence models, the zonal k–ε model produces the highest levels near wall turbulence energy, whilst the non-linear model returns the lowest. As a result, among all turbulence models, the zonal k–ε model results in the steepest near-wall temperature gradients (see Figure 12) which are consistent with highest heat transfer levels returned with this model in Figure 9.

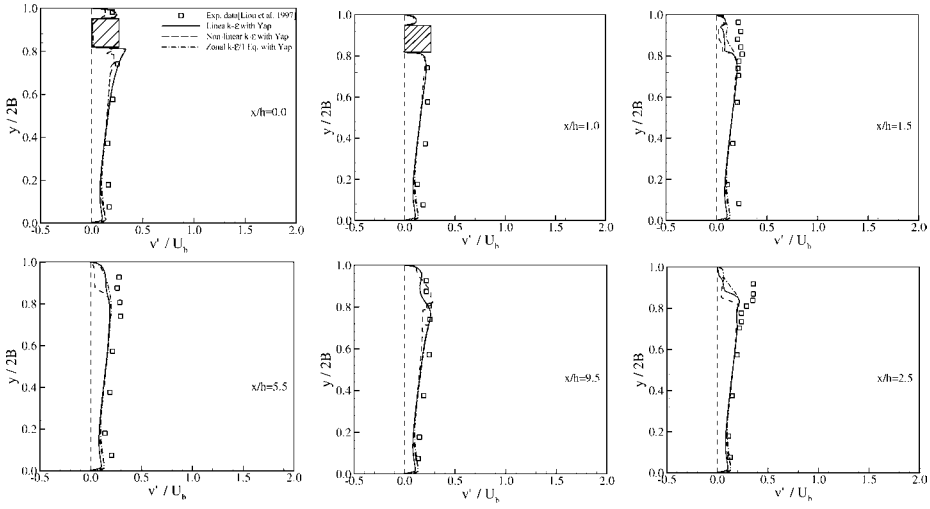

Figure 8.
cross-stream turbulent intensity profiles for air flow through the channel with detached ribs on one wall (case a)

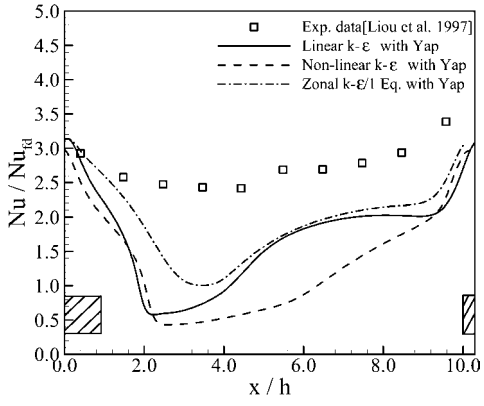

Figure 9.
Distribution of Nusselt number ratio (Nu/Nu_{fd}) for air flow through the channel with detached ribs on one wall (case a)

For the second test case (channel with ribs detached from both principal walls), the predicted Nusselt number ratios (Nu/Nu_{fd}) and the distribution of the near-wall turbulence energy returned by the turbulence models are presented in Figures 13 and 14, respectively. It is clear that there is a close correlation between the local Nusselt number and the near-wall turbulent kinetic energy. Both Nu/Nu_{fd} and k distributions reach a peak at a location about 0.4 rib-height downstream of the channel inlet. Subsequently, both Nu/Nu_{fd} and $\sqrt{k}/U_b$ drop along the channel until the vicinity of the downstream rib where both increase again. Concerning the performance of the turbulence models, it is noted that all three low-Re k–ε models returned similar heat transfer predictions. Although all three turbulence models reproduce the distribution of the local heat transfer coefficient, similar to the first case, they somewhat underpredicted the measured data. Here again the zonal k–ε model produces the best heat transfer predictions, while the linear and non-linear models return similar and lower levels for local Nusselt number.

For the channel with alternative attached-detached ribs, the predicted Nusselt number ratios are compared in Figure 15 with the experimental data of Tsia and Hwang (1999). In the first half of the channel (i.e. between the first detached rib and the

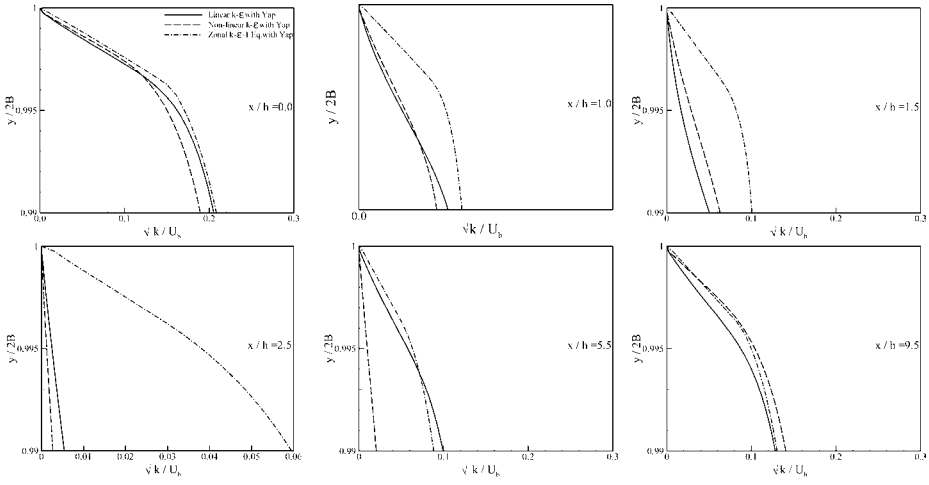

Figure 10.
Near-wall turbulent kinetic energy profiles for air flow through the channel with detached ribs on one wall (case a)

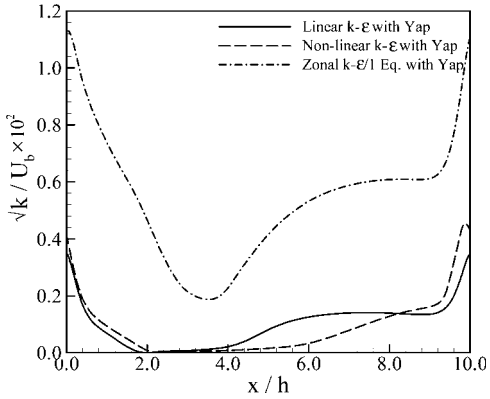

Figure 11.
Distribution of turbulent kinetic energy (k) for air flow through the channel with detached ribs on one wall (case a)

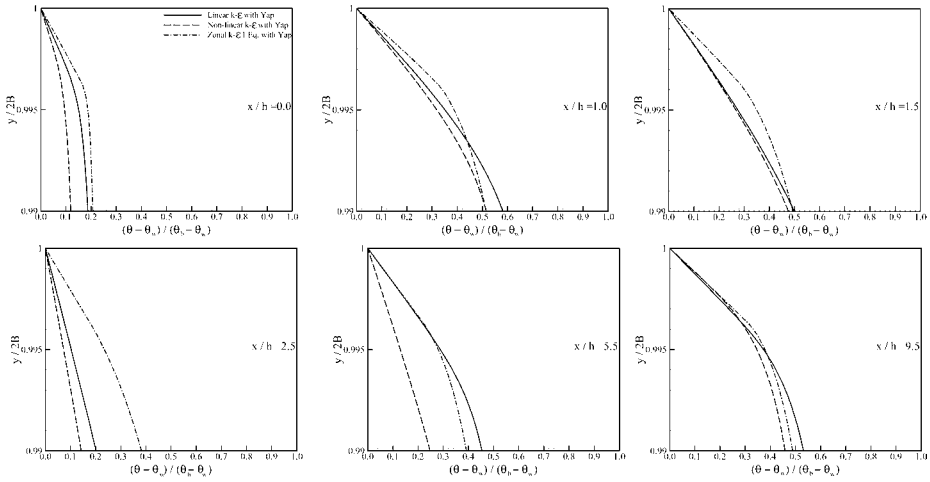

Figure 12.
Near-wall temperature profiles for air flow through the channel with detached ribs on one wall (case a)

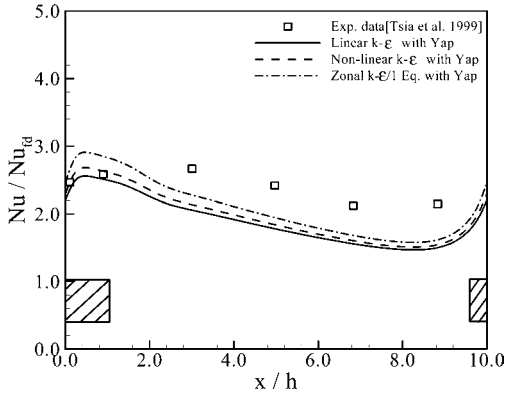

Figure 13.
Distribution of Nusselt number ratio (Nu/Nu_{fd}) for air flow through the channel with detached ribs on two walls (case b)

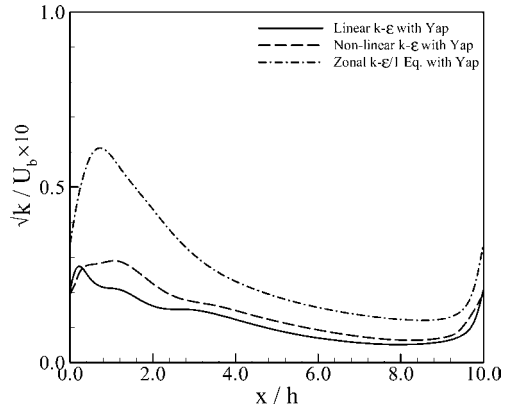

Figure 14.
Distribution of turbulent kinetic energy (k) for air flow through the channel with detached ribs on two walls (case b)

second attached rib) all turbulence models overpredict the experimental data and subsequently underestimate them. In the second half of the interval (downstream of the attached rib) all three turbulence models overestimated the measured data, though produced somewhat better thermal predictions. As found for previous cases, here again the zonal k–ε model returns the best heat transfer predictions and the linear and non-linear models produce similarly worst heat transfer levels.

To explain differences in thermal predictions of turbulence models, the predicted near-wall turbulence energy of the models is compared in Figure 16. As can be clearly seen there is close correlation between the distributions of local Nusselt number shown in Figure 15 and turbulence energy. In general the zonal k–ε model predicts the highest levels of turbulence energy while the linear and non-linear models produce the lowest. Thus, it can be concluded that the differences in thermal prediction of turbulence models used in the current study is due to near-wall turbulence energy predictions of these models.

The differences between the predictions may be due to the fact that flow in channels with detached ribs is unsteady. It is expected that the unsteady computations produce more accurate flow and thermal predictions. This suggests that the more expensive time-dependent approaches such as unsteady RANS or LES may be necessary. The present set of heat and fluid flow comparisons establishes a base-level against which similarly comprehensive comparisons that involve more advanced approaches can be assessed.

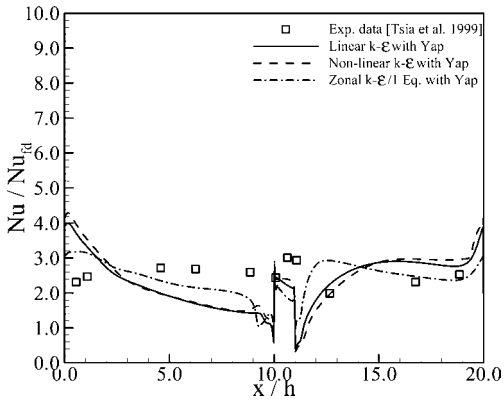

Figure 15.
Distribution of Nusselt number ratio (Nu/Nu_{fd}) for air flow through the channel with attached-detached ribs on two walls (case c)

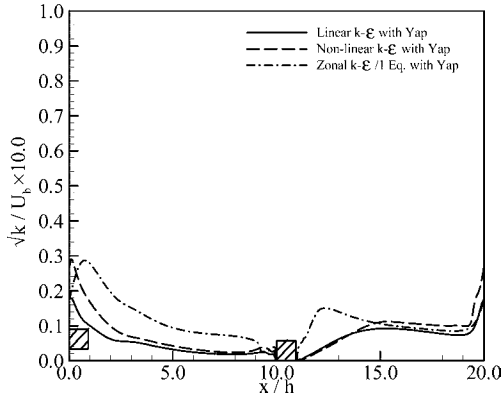

Figure 16.
Distribution of turbulent kinetic energy (k) for air flow through the channel with alternative attached-detached ribs on two walls (case c)

7. Conclusions

In this paper, the zonal and the linear and non-linear low-Reynolds number k–ε models have been employed to investigate fluid flow and heat transfer through channels roughened with an array of either detached or alternative attached-detached ribs. It was found that all low-Re k–ε models are able to produce reasonable velocity predictions in the core region of channels but fail to predict correct levels for velocity filed in the vicinity of the ribbed wall. While all models produce correct levels for the cross-stream turbulence intensity in the core region, the stream-wise turbulence intensity is seriously underpredicted by all the turbulence models. All three turbulence models seriously underpredict the velocity and turbulence levels in the region close to the ribbed wall. For the channels with detached ribs, all turbulence models underpredict the Nusselt levels. For the channel with alternative attached-detached ribs, all turbulence models produce poor heat transfer results in the first half of the channel, whilst in the second half, the heat transfer predictions of the turbulence models are in good overall agreement with the measurements. In general, it can be concluded that among turbulence models examined, the zonal k–ε model produces the best heat transfer predictions. It is believed that one reason of discrepancies between the heat transfer predictions and measurements is the fact that actual flow in channels with the detached ribs is unsteady. Thus, steady flow computations cannot fully capture flow and thermal field characteristics.

References

Craft, T.J., Iacovides, H. and Yoon, J.H. (1999), "Progress in the use of non-linear two-equation models in the computation of convective heat transfer in impinging and separated flows", *Journal of Flow Turbulence and Combustion*, Vol. 63, pp. 59-80.

Craft, T.J., Launder, B.E. and Suga, K. (1993), "Extending the applicability of eddy-viscosity models through the use of deformation invariants and non-linear elements", *Proceedings of 5th International Symposium, Refined Flow Modeling and Turbulence Measurements, Paris*, pp. 125-32.

Durbin, P.A. (1995), "Separated flow computations with the k–ε–v^2 model", *Journal AIAA*, Vol. 33 No. 4, pp. 659-64.

Han, J.C, (1988), "Heat transfer and friction characteristics in rectangular channels with rib tabulator", *Journal of Heat transfer*, Vol. 110, pp. 91-8.

Hsieh, K.J. and Lien, F.S. (2005), "Conjugate turbulent forced convection in a channel with an array of ribs", *International Journal of Numerical Methods for Heat and Fluid Flow*, Vol. 15 No. 5, pp. 462-82.

Iacovides, H. and Raisee, M. (1999), "Recent progress in the computation of flow and heat transfer in internal cooling passages of gas turbine blades", *International Journal of Heat and Fluid Flow*, Vol. 20, pp. 320-28.

Iacovides, H. and Raisee, M. (2000), "Computation of flow and heat transfer in two-dimensional rib-roughened passages, using low-Reynolds-number turbulence models", *International Journal of Numerical Methods for Heat and Fluid Flow*, Vol. 11, pp. 138-55.

Iacovides, H. and Raisee, M. (2008), "Turbulent flow and heat transfer in stationary and rotating cooling passages with inclined ribs on opposite walls", *International Journal of Numerical Methods for Heat and Fluid Flow*, Vol. 18, pp. 258-78.

Jones, W.P. and Launder, B.E. (1972), "The prediction of laminarization with a two-equation model of turbulence", *International Journal of Heat Mass Transfer*, Vol. 15, pp. 301-14.

Launder, B.E. and Sharma, B.I. (1974), "Application of the energy-dissipation model of turbulence to the calculation of flow near a spinning disk", *Letters in Heat Mass Transfer*, Vol. 1, pp. 131-38.

Lee, B.K., Cho, N.H. and Choi, Y.D. (1988), "Analysis of periodically fully-developed turbulent flow and heat transfer by k–ε equation model in artificially roughened annulus", *International Journal of Heat Mass Transfer*, Vol. 31, pp. 1797-806.

Lin, C.A. and Hwang, C.B. (1998), "Improved low-Reynolds-number k–ε model based on direct numerical simulation data", *Journal AIAA*, Vol. 36 No. 1, pp. 38-43.

Liou, T.M. and Hwang, J.J. (1992), "Turbulent transfer augmentation and friction in periodic fully developed channel flows", *Journal of Heat Transfer*, Vol. 114, pp. 56-64.

Liou, T.M. and Wang, W.B. (1995), "Laser holographic interferometery study of developing heat transfer in a duct with a detached rib array", *International Journal of Heat Mass Transfer*, Vol. 38, pp. 91-100.

Liou, T.M., Hwang, J.J. and Chen, S.H. (1993), "Simulation and measurement of enhanced turbulent heat transfer in a channel with periodic ribs on one principal wall", *International Journal of Heat Mass Transfer*, Vol. 36, pp. 507-17.

Liou, T.M., Yang, C.P. and Lee, H.L. (1997), "LDV measurements of spatially periodic flow over detached solid-rib array", *Journal of Fluids Engineering*, Vol. 119, pp. 383-89.

Nonino, C. and Comini, G. (2002), "Convective heat transfer in ribbed square channels", *International Journal of Numerical Methods for Heat and Fluid Flow*, Vol. 12 No. 5, pp. 610-28.

Raisee, M., Noursadeghi, A. and Iacovides, H. (2004), "Application of non-linear k–ε in prediction of convective heat transfer through ribbed passages", *International Journal of Numerical Methods for Heat and Fluid Flow*, Vol. 14, pp. 285-304.

Rhie, C.M. and Chow, W.L. (1983), "Numerical Study of the turbulent flow past an airfoil with trailing edge separation", *Journal AIAA*, Vol. 21, pp. 1525-32.

Suga, K. (1995), "Development and application of a non-linear eddy viscosity model sensitized to stress and strain invariants", PhD thesis, Faculty of Technology, University of Manchester, Manchester.

Tsia, J.P. and Hwang, J.J. (1999), "Measurements of heat transfer and fluid flow in a rectangular duct with alternative attached-detached rib-arrays", *International Journal of Heat Mass Transfer*, Vol. 42, pp. 2072-83.

Tsia, W.B. and Lin, W.W. (2000), "Computation of enhanced turbulent heat transfer in a channel with periodic ribs", *International Journal of Numerical Methods for Heat and Fluid Flow*, Vol. 10 No. 1, pp. 47-66.

Webb, R.L., Eckert, E.R.G. and Goldstein, R.J. (1971), "Heat transfer and friction in tubes with repeated-rib roughness", *International Journal of Heat and Mass transfer*, Vol. 14, pp. 601-17.

Woolfshtein, M. (1969), "The velocity and temperature distribution in one-dimensional flow with turbulence augmentation and pressure gradient", *International Journal of Heat and Mass Transfer*, Vol. 12, p. 301.

Wu, H. and Perng, S. (2004), "Turbulent flow and heat transfer enhancement of mixed convection over heated blocks in a channel", *International Journal for Numerical Methods in Heat and Fluid Flow*, Vol. 15 No. 2, pp. 205-25.

Yap, C.R. (1987), "Turbulent heat and momentum transfer in recirculating and impinging flows", PhD thesis, Department of Mechanical Engineering, Faculty of Technology, University of Manchester, Manchester.

Corresponding author
Mehrdad Raisee can be contacted at: mraisee@ut.ac.ir